Session 0A9
Advances in Integral Equation Techniques for Planar Circuits

Conformal Meshing in FFT Based EM Analysis

J. C. Rautio
Sonnet Software, Inc., USA

Shielded planar EM analysis is based on the FFT. This means it has extremely high accuracy and dynamic range (due to the complete absence of numerical integration), but it also analyzes a circuit based on a fine underlying FFT mesh. While the FFT mesh can be even finer than the pixels on a typical computer screen, it does result in more difficulty in analyzing non-Manhattan geometries. Conformal mesh eliminates this problem for a broad class of non-Manhattan geometries including curved transmission lines, like circular spiral inductors. The nature of this conformal meshing is described and examples are given. Complicated circuits with curving transmission lines can now be analyzed quickly even if they can not be analyzed at all (to the same degree of error) on any other EM tool of any kind.

An Analysis of Coaxial Line Slot antenna for Hyperthermia Treatment by Spectral Domain Approach

T. Nakata, **H. Yoshitake**, **K. Wakino**, **Y.-D. Lin**, **and T. Kitazawa**
Ritsumeikan University, Japan

Abstract—An extended spectral domain approach (ESDA) is applied to evaluate the scattering parameter of laterally slotted coaxial antenna for hyperthermia treatment. The results calculated by ESDA are in good agreement with that by Finite Element Method (FEM) simulation. Computational labor of the present method is far lighter than that of FEM, and the method is suitable for the iterative computation that is required for the optimization of antenna design. The present method can afford to consider the effect of the metallization thickness in the outer conductor.

1. Introduction

In the fields of medical application, microwave is utilized for various purposes in the examining and treatment equipment [1]. The characteristics of coaxial line slot antenna for microwave hyperthermia applicators have been investigated [2]. This treatment thrusts a coaxial line applicator into the affected cancer part, heats up selectively the affected area and fixes the cancer cells. The currently used coaxial line applicator is not optimized in the point of view of impedance matching between applicator and human tissue, so that the radiation efficiency into the affected area is not good. In this paper, we analyze the radiation characteristics of applicator using efficient simulation technique and proposed the optimized design that presents high radiation efficiency.

The formulation procedure utilized in this paper is based on the extended spectral domain approach (ESDA). This procedure can afford to consider the effect of thickness of outer conductor of coaxial cable. The results calculated by ESDA are compared with that by FEM simulation and excellent agreement have been obtained between both results.

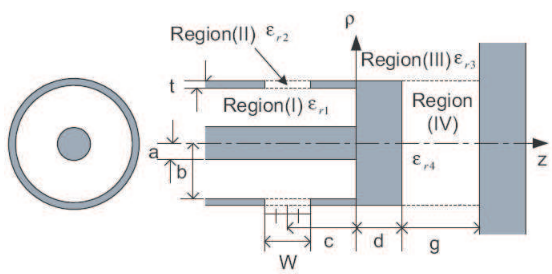

Figure 1: Schematic structure of coaxial line slot antenna.

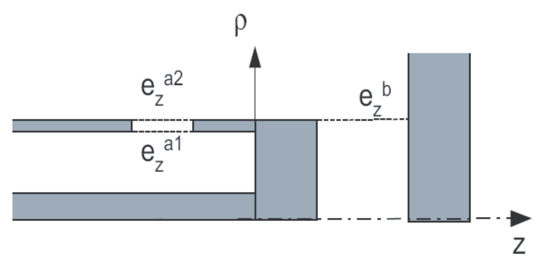

Figure 2: Aperture electric fields.

2. Theory

Figure 1 shows the schematic structure of coaxial line slot antenna whose outer conductor has finite thickness t and has a ring slot of W in width cut laterally near the termination. A perfect electric conductor (PEC) sheet is introduced for convenience of analysis in the position apart g from the tip of coaxial line. It is assumed that the relative complex permittivity of material in each region is ϵ_{r1}, ϵ_{r2}, ϵ_{r3}, ϵ_{r4}, respectively. The radiation characteristics of coaxial line slot antenna are analyzed based on the extended spectral domain approach (ESDA) [3]. In the procedure, first the aperture fields are introduced in the aperture of outer conductor designated as e_z^{a1}(at $\rho = b$), and e_z^{a2}(at $\rho = b + t$) (Fig. 2), respectively. Whole analytic space is divided into four regions, that is, region I ($a \leq \rho \leq b$, $-\infty \leq z \leq 0$), region II ($b \leq \rho \leq b + t$, $-c - w/2 \leq z \leq -c + w/2$), region III ($b + t \leq \rho \leq r$, $-\infty \leq z \leq d + g$), and region IV ($0 \leq \rho \leq b + t$, $d \leq z \leq d + g$), as shown in Fig. 1. These regions can be treated independently resorting to equivalence theorem, and the electromagnetic fields in each region are Fourier transformed with respect to the z-direction. When the dominant TEM mode

$$E_\rho = \frac{E_0}{\rho}\exp(-jk_1 z), \quad H_\phi = \sqrt{\frac{\epsilon_{r1}\epsilon_0}{\mu_0}}\frac{E_0}{\rho}\exp(-jk_1 z) \quad (a \leq \rho \leq b) \tag{1}$$

enters the coaxial line slot antenna, there exist the incident and the scattered waves in region (I) and total

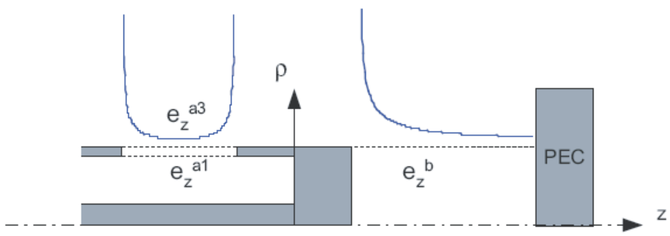

Figure 3: Edge singularities in aperture fields.

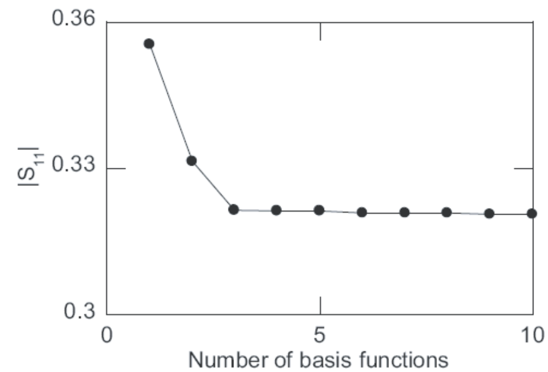

Figure 4: Convergence of the reflection coefficients with respect to number of basis functions. $a = 0.24\,\text{mm}$, $b = 0.8\,\text{mm}$, $c = 2.5\,\text{mm}$, $d = 5.0\,\text{mm}$, $w = 2.0\,\text{mm}$, $t = 0.1\,\text{mm}$, $\epsilon_{r1} = 2.1 - j0.0005$, $\epsilon_{r2} = \epsilon_{r3} = \epsilon_{r4} = 43 - j12.38$, $f = 2.45\,\text{GHz}$.

electromagnetic fields are expressed by Fourier integrals as,

$$\begin{aligned} E_\rho^{(I)}(\rho,z) &= -j\frac{2E_0}{\rho}\sin(k_1 z) + \sqrt{\frac{2}{\pi}}\int_{-\infty}^{0}\tilde{E}_\rho^{(I)}(\rho)\sin(\alpha_1 z)d\alpha_1, \\ E_z^{(I)}(\rho,z) &= \sqrt{\frac{2}{\pi}}\int_{-\infty}^{0}\tilde{E}_z^{(I)}(\rho)\cos(\alpha_1 z)d\alpha_1, \\ E_\phi^{(I)}(\rho,z) &= \sqrt{\frac{\epsilon_{r1}\epsilon_0}{\mu_0}}\frac{2E_0}{\rho}\cos(k_1 z) + \sqrt{\frac{2}{\pi}}\int_{-\infty}^{0}\tilde{H}_\phi^{(I)}(\rho)\cos(\alpha_1 z)d\alpha_1 \end{aligned} \tag{2}$$

Similar expressions are available in region (III). The electromagnetic fields in regions (II) and (IV) are expressed by Fourier series instead of Fourier integrals to satisfy the boundary conditions on the side walls. Fields in regions (II) are expressed as

$$\begin{aligned} E_\rho^{(II)}(\rho,z) &= \sum_{n=1}^{\infty}\tilde{E}_\rho^{(II)}(\rho)\sin\alpha_2(z+c+\frac{W}{2}), \quad E_z^{(II)}(\rho,z) = \sum_{n=0}^{\infty}\tilde{E}_z^{(II)}(\rho)\cos\alpha_2(z+c+\frac{W}{2}), \\ H_\phi^{(II)}(\rho,z) &= \sum_{n=0}^{\infty}\tilde{H}_\phi^{(II)}(\rho)\cos\alpha_2(z+c+\frac{W}{2}), \quad \alpha_2 = \frac{n\pi}{W}. \end{aligned} \tag{3}$$

And similar expressions are available in region (IV).

These expressions of electromagnetic fields are substituted into Maxwells field equations. The general solutions of the transformed field equations can be expressed in terms of Bessel functions and Neumann functions in regions (I), (II) and (IV), and in terms of second kind of Hankel functions in region (III) as

$$\tilde{H}_\phi^{(i)}(\alpha_i;\rho) = A^{(i)}J_1(\xi_i\rho) + B^{(i)}N_1(\xi_i\rho) \quad \text{in regions(I), (II) and (IV)} \tag{4}$$

$$\tilde{H}_\phi^{(III)}(\alpha_3;\rho) = C^{(III)}H_1^{(2)}(\xi_3\rho) \quad \text{in regions(III)} \tag{5}$$

where $A_{(i)}$, $B_{(i)}$ and $C^{(III)}$ are unknown constants and $\xi_i = \sqrt{\omega^2\epsilon_{ri}\epsilon_0\mu_0 - \alpha_i^2}$. These unknown constants can be related to the aperture fields e_z^{a1}, e_z^{a2} and e_z^{b} by applying the continuities of electric fields at interfaces. Then the electromagnetic fields in each region are expressed in terms of the aperture fields, for example,

$$H_\phi^{(I)}(\rho,z) = \sqrt{\frac{\epsilon_{r1}\epsilon_0}{\mu_0}}\frac{2E_0}{\rho}\cos(k_1 z) + \int_{z'=-c-W/2}^{-c+W/2} Y^{(I)}(\rho,z|\rho'=b,z')e_z^{a1}(z')dz' \quad \text{in region(I)} \tag{6}$$

where $Y^{(I)}$ is the Green's function and it can be derived easily in the transformed domain. Similar expressions are derived in other regions, which relate the fields to the involved aperture fields. The remaining boundary conditions, i.e., the continuity of the magnetic field at the interfaces between adjacent regions, are applied to obtain a set of the integral equations on the aperture fields. The aperture fields can be determined by applying

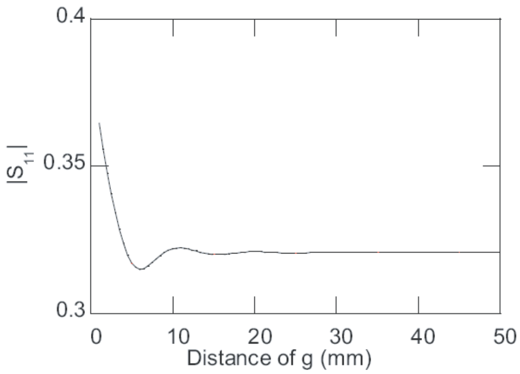

Figure 5: Convergence of reflection coefficients with respect to the distance of g. $a = 0.24$ mm, $b = 0.8$ mm, $c = 2.5$ mm, $d = 5.0$ mm, $w = 2.0$ mm, $t = 0.1$ mm, $\epsilon_{r1} = 2.1 - j0.0005$, $\epsilon_{r2} = \epsilon_{r3} = \epsilon_{r4} = 43 - j12.38$, $f = 2.45$ GHz.

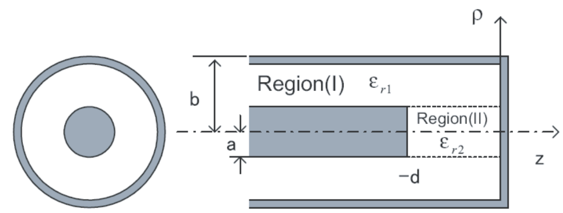

Figure 6: Gap discontinuity in coaxial line.

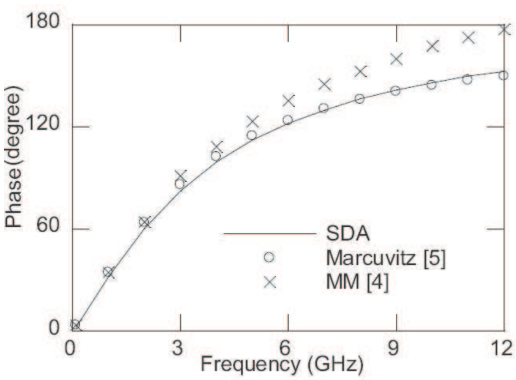

Figure 7: Phase variation of the reflection versus the frequency. $a = 3.10$ mm, $b = 7.14$ mm, $d = 0.57$ mm, $\epsilon_{r1} = \epsilon_{r2} = 2.1$.

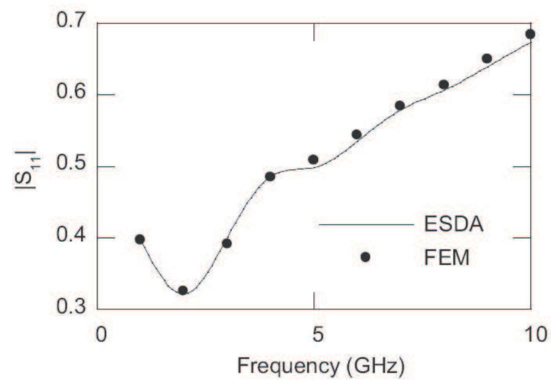

Figure 8: Frequency dependency of reflection coefficients of coaxial line slot antenna. $a = 0.24$ mm, $b = 0.8$ mm, $c = 2.5$ mm, $d = 5.0$ mm, $w = 2.0$ mm, $t = 0.1$ mm, $\epsilon_{r1} = 2.1 - j0.0005$, $\epsilon_{r2} = \epsilon_{r3} = \epsilon_{r4} = 43 - j12.38$.

the Galerkin's procedure to these coupled integral equations, and the scattering parameter (complex reflection constant) S_{11} are obtained by taking the inner product between the aperture field e_z^{a1} and the eigen function of coaxial line.

3. Numerical Procedure and Result

The numerical procedure is based on Galerkin's procedure, and the unknown electric aperture fields e_z^{a1}, e_z^{a2} and e_z^b are expanded in terms of the appropriate basis functions,

$$e_z^i(z) = \sum_{k=1}^{N} a_k^i f_k^i(z) \tag{7}$$

The basis functions $f_k^i(z)$ are chosen taking the edge singularities near conductor edge into consideration (Fig. 3),

$$f_k^{a1}(z) = f_k^{a2} K(z) = \frac{T_{k-1}\{\frac{2}{W}(z+c)\}}{\sqrt{1-\{\frac{2}{W}(z+c)\}^2}}, \quad f_k^b(z) = \frac{T_{2(k-1)}\{\frac{1}{g}(z-d-g)\}}{\sqrt{1-\{\frac{1}{g}(z-d-g)\}^2}} \tag{8}$$

where $T_k(x)$ is Chebyshev polynomials of the first kind.

Preliminary computations are carried out to investigate the convergence of the reflection coefficients with respect to the number of basis functions. This method was settled by a little number of basis functions as shown in Fig. 4, and $N = 8$ is used in the following computations. Fig. 5 examines the effect of the fictious perfect electric conductor sheet placed at distance g ahead the tip of coaxial line slot antenna (Fig. 1). The influence of the conductor sheet decreases rapidly with g, and the sufficient spacing $g = 40$ mm is chosen in the following simulations.

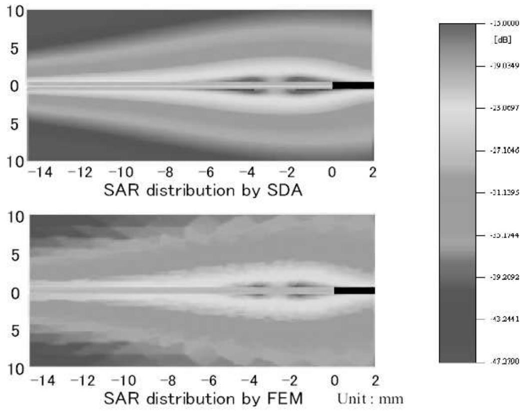

3

Figure 9: SAR distribution of coaxial line slot antenna.

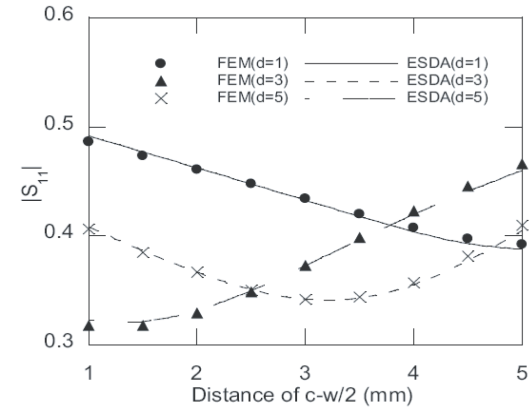

Figure 10: Variation of the reflection versus the slot position. $a = 0.24\,\text{mm}$, $b = 0.8\,\text{mm}$, $w = 2.0\,\text{mm}$, $t = 0.1\,\text{mm}$, $\epsilon_{r1} = 2.1 - j0.0005$, $\epsilon_{r2} = \epsilon_{r3} = \epsilon_{r4} = 43 - j12.38$, $f = 2.45\,\text{GHz}$.

To author's knowledge there is no published theoretical result to permit direct comparison with the present method for the reflection characteristics of coaxial line slot antenna. We apply the present method to analyze the gap discontinuity in the inner conductor of shorted coaxial line (Fig. 6) to show the validity of the method. The formulation procedures are similar to those explained above and also the similar basis functions (8) are used in the numerical computation. Fig. 7 shows the phase variation of the reflection coefficient versus the frequency, comparing the results by mode-matching method [4] and Marcuvitzs analytical results [5]. Our results are in good agreement with [5] for wide frequencies.

Figure8 shows the frequency dependency of reflection coefficients of the coaxial line slot antenna (applicator) thrust into the liver. The figure includes the values by FEM for comparison, and excellent agreement is observed between both methods over wide frequencies. Fig. 9 shows the SAR distribution calculated by both methods at $f = 2.45\,\text{GHz}$.

The present method is numerically efficient and is suitable for the optimization of the coaxial line applicator, which requires the iterative computations. Fig. 10 shows the optimization of coaxial line by changing a slot position when the operation frequency is 2.45 GHz. The optimal value at this condition takes the reflective coefficient 0.32 at $c - w/2 = 1.5\,\text{mm}$ and $d = 5\,\text{mm}$. This figure also includes the values by FEM and again good agreement is confirmed, although FEM calculations are time consuming and are presented only at discrete frequencies.

4. Conclusion

In this paper, we proposed the novel analyzing technique for the coaxial line slot antenna by ESDA, and carried out extraction of scattering parameters. This method can take the thickness effect of outer conductor into consideration. This method also secures the high accuracy by considering the singularities of fields near the conductor edge properly. The computational labor of the new method is far lighter than that of FEM, so that novel method is suitable for the time consuming iterative computation such as optimization procedure of antenna design.

REFERENCES

1. Sterzer, S., "Microwave medical devices," *IEEE Microwave Magazine.*, Vol. 3, 65–70, March 2002.
2. Saito, K., Y. Hayashi, H. Yoshimura, and K. Ito, "Heating characteristics of array applicator composed of two coaxial-slot antennas for microwave coagulation therapy," *IEEE Trans. Microwave Theory Tech.*, Vol. 48, 1800–1806, November 2000.
3. Kitazawa, T., "Nonreciprocity of phase constants, characteristic impedances and conductor losses in planar transmission lines with layered anisotropic media," *IEEE Trans. Microwave Theory Tech.*, Vol. 43, 445–451, February 1995.
4. Eom, H. J., Y. C. Noh, and J. K. Park, "Scattering analysis of a coaxial line terminated by a gap," *IEEE Microwave Guided Wave Lett.*, Vol. 8, 218–219, June 1998.
5. Marcuvitz, N., *Waveguide Handbook*, New York: McGraw-Hill, 178, 1951.

Spectral Domain Analysis of Coupled Microstrip Using Spheroidal Wave Functions with Edge Conditions

C. A. Carter
Stevens Institute of Technology, USA

An analysis of coupled microstrip transmission lines using spheroidal wave functions and the spectral domain method will be presented. In the spectral domain method, the electromagnetic field equations and boundary conditions are formulated in the spectral, or Fourier transform, domain. This formulation is used to derive an equation that expresses the Fourier transform of the electric field in terms of the current distribution on the microstrip. Galerkin's moment method is then applied to yield a system of equations that can be used to solve for unknown propagation constants as a function of frequency.

The current distribution on microstrip is modeled as an expansion of known basis functions with unknown coefficients. Walsh functions, sinusoidal functions, sinusoidal functions with edge conditions and Chebyshev polynomials with edge conditions have been utilized as basis functions in prior research. Functions that incorporate the microstrip edge conditions more effectively model the current on the microstrip and require fewer terms in the current expansion. Previous research at Stevens Institute of Technology has utilized spheroidal wave functions to model the current distribution on single microstrip transmission lines. These functions were shown to model the current over a broad frequency range and required fewer expansion terms than other previously used basis functions.

For this presentation, the work carried out utilizing spheroidal wave functions in the analysis of single microstrip lines is extended to coupled microstrip. A brief overview of the theory of spheroidal wave functions will be included but the primary focus will be on practical issues of computation related to their use in the analysis of both single and coupled microstrip. Chebyshev polynomials with edge conditions have previously been used to model the current on coupled microstrip over a large frequency range. Preliminary results demonstrate that fewer spheroidal wave functions than Chebyshev polynomials are needed to compute the propagation constant as a function of frequency. Propagation constants computed for a range of frequencies and strip separation values are investigated.

Application of the Space Domain MoM Technique to the Analysis of Planar Guiding Structures

M. B. Ben Salah, **M. Souden**, **A. B. Kouki**, **and A. Samet**
Ecole Polytechnique de Tunisie, Tunisia

Integral equation methods are widely recognized as efficient techniques for studying the propagation characteristics of planar structures. In these techniques, the Method of Moments in the spectral domain is typically used since the Green's functions can be obtained in closed form. This approach has been shown to be quite effective for the modeling of planar guiding structures and is behind several empirical models used today in many commercial microwave CAD tools. Nevertheless, this approach requires the evaluation of infinite integrals with oscillating and slowly decaying integrands, for open structures, and infinite series for shielded ones. To circumvent this problem, a space domain formulation of the Method of Moments, widely used to characterize arbitrary planar structures and discontinuities, is proposed for the analysis of guiding structures. The closed form expressions of the Green's functions for the vector and scalar potentials in the space domain are found through the application of the Generalized Pencil of Functions (GPOF) method to the one dimensional case. In such a case, we show that the passage from the spectral to the space domain results in a simplified closed form expression in terms of Bessel functions of the second kind. This new formulation is applied to a microstrip line and the results are compared to other models.

On the Limitations of the Space Domain Formulation of the MoM Method for Planar Circuits

K. Kochlef, A. B. Kouki, and A. Samet
Ecole Polytechnique de Tunisie, Tunisie

The Method of Moments (MoM) is arguably the most well suited technique for the analysis of planar circuits. This technique has been traditionally formulated in the spectral domain, since it is only in this domain that the Green's functions can be determined exactly. However, the spectral domain formulation suffers from several limitations, particularly for open structures, that make its implementation and use difficult and the required computational resources high. In light of this, substantial research effort has been invested in developing a space domain alternative whereby an approximate space domain Green's function is derived from its spectral domain counterpart and used in space domain formulation of the MoM technique. Therefore, the accuracy of this technique depends on that of the space domain Green's function.

In this paper, we present a systematic investigation of the accuracy of the space domain MoM technique applied to single layer planar circuits with the aim of establishing its limitations and determining its zones of applicability. The study covers a wide range of parameters, including frequency, cell spacing, dielectric constant values and substrate height. We also examine the impact of varying the parameters of the generalized pencil of function (GPOF) technique, used to determine the space domain Green's function, on the precision of the technique and its zones of applicability. Finally we discuss potential remedies to overcome the limitation of the space domain techniques.

REFERENCES

1. Aksun, M. I., "A robust approach for the derivation of closed-form Green's function for a general microstrip geometry," *IEEE Trans. Microwave Theory Tech.*, Vol. 44, 651–658, May 1996.
2. Shuley, N. V., R. R. Boix, F. Medina, and M. Horno, "On the fast approximation of Green's functions in MPIE formulations for planar layered media," *IEEE Transactions on Microwave Theory and Techniques*, Vol. 50, No. 9, 2185–2112, September 2002.
3. Sarkar, T. K. and O. Pereira, "Using the matrix pencil method to estimate the parameters of a sum of complex exponentials," *IEEE Trans. Antennas and Propagation Magazine*, Vol. 37, 48–55, February 1995.
4. Alatan, L., M. I. Aksun, K. Mahadevan, and M. T. Birand, "Analytical evaluation of the MOM matrix elements," *IEEE Transactions on Microwave Theory and Techniques*, Vol. 44, No. 4, April 1996.

Critical Study of DCIM, and Development of Efficient Simulation Tool for 3D Printed Structures in Multilayer Media

M. I. Aksun and T. Onal
Koc University, Turkey

Abstract—Since the discrete complex image method (DCIM) has been widely used in conjunction with the Method of Moments (MoM) to efficiently analyze printed structures, some lingering issues related to the implementation of DCIM and their brief clarifications are first reviewed. Then, an efficient and rigorous electromagnetic simulation algorithm, based on the combination of MoM and DCIM, is proposed and developed for the solution of mixed-potential integral equation (MPIE) for printed structures with multiple vertical strips in multilayer media. The algorithm is possibly the most efficient approach to handle multiple vertical conductors, even spanning more than one layer, in printed circuits.

1. Introduction

Spatial-domain method of moments (MoM) is a widely used technique for the solution of mixed-potential integral equation (MPIE) for printed geometries in multilayer planar media [1], thanks to the introduction of an efficient closed-form approximation method [2] and its improved versions of the spatial-domain Green's functions [3, 4]. This approach, known as discrete complex image method (DCIM), basically approximates the spectral-domain Green's functions in terms of complex exponentials, and then casts the integral representations of the spatial-domain Green's functions into closed-form expressions via Sommerfeld identity [5]. Although DCIM is quite robust and works well to get the closed-form Green's functions, it has some limitations in the form of a limited range of validity depending upon the implementation of the method.

Some issues originating from the implementation of DCIM are discussed and possible clarifications are provided in Section 2. In Section 3, application of the closed-form Green's functions in conjunction with the spatial-domain MoM is reviewed, with the emphasis given to efficient handling of multiple vertical conductors. Finally, conclusions are provided in Section 4.

2. Discussions on Closed-form Green's Functions

It is well known that spectral-domain Green's functions can be written analytically in planar multilayer media, and their spatial-domain counterparts can be obtained from the inverse Hankel transform of the spectral-domain Green's functions [4, 6], as

$$G = \frac{1}{4\pi} \int_{SIP} dk_\rho k_\rho H_0^{(2)}(k_\rho \rho) \widetilde{G}(k_\rho) \tag{1}$$

where $k_\rho^2 = k_x^2 + k_y^2$, ρ is the variable in cylindrical coordinate system, G and $\widetilde{G}$ are Green's functions in the spatial and spectral domain, respectively, $H_0^{(2)}$ is the Hankel function of the second kind and SIP is the Sommerfeld integration path. Since the integrand usually exhibits oscillatory nature and slow convergence, rendering the transformation computationally very expensive, spectral-domain Green's functions can be approximated by complex exponentials, via the generalized pencil-of-function (GPOF) method [6], to obtain closed-form expressions from the inverse Hankel transform. Since the crucial step in this approach is the approximation of the spectral-domain Green's functions, which is detailed in [3, 4], discussions on the accuracy of the method for large distances have concentrated mainly on the approximation procedure, because the resulting closed-form Green's functions are, in general, accurate enough for distances as far as $k_0\rho = 20 - 30$ ($\rho/\lambda = 3 - 4$), beyond which they may deteriorate significantly.

In the literature, there were basically three attributable sources of problems in the implementation of DCIM: (i) not extracting the quasi-static terms, (ii) introducing a wrong branch point in the process of approximation, and (iii) not extracting the surface wave poles (SWP). In the original implementation of DCIM, as introduced in [2], there were only one level of approximation, and it was necessary to extract the quasi-static terms to make the remaining portion of the spectral-domain Green's functions converge to zero for large k_ρ values. However, with the introduction of two-level and multi-level approximation algorithms [3, 7], the necessity of finding the quasi-static terms and their extraction before the approximation has been eliminated. The issue of introducing wrong branch point originates from the following observations: spectral-domain Green's functions, when the source is in a bounded layer, have no branch point at $k_\rho = k_s$, although they have k_{zs} term in the denominator, where k_s is the wave number of the source layer; and the approximating exponentials with k_{zs} factor in the denominator seem to have branch point at $k_\rho = k_s$. However, one should note that the exponential approximation is always performed over the deformed path of SIP and the function to be approximated over this path is single valued with the right choice of the branch. Therefore, the resulting exponentials divided by k_{zs} is a singlevalued function with this right choice of the branch. The last problem concerning the SWPs is inherent to the approach unless the SWP contributions are totally extracted from the functions to be approximated. The detailed discussions on these issues and some clarifications can be found in [4].

3. MoM-DCIM Application for Multiple Vertical Strips

In the analysis of printed geometries with multiple vertical strips, a method based on MoMDCIM is employed, as proposed in [7], and it is extended to efficiently handle multiple vertical strips. The algorithm and its efficient handling of multiple vertical strips can be described by examining one of the inner-product terms in the MoM matrix entries, as follows:

$$\left\langle \frac{\partial}{\partial x} T_x(x,y),\, G_z^q * \frac{\partial}{\partial z} B_z(y,z) \right\rangle = \iint dxdy \frac{\partial}{\partial x} T_x(x,y) \cdot \int dy' B_z(y') \int dz' \frac{\partial}{\partial z'} B_z(z') G_z^q(x-x', y-y', z, z') \quad (2)$$

where $T_x(x,y)$ and $B_z(x,y)$ are the testing and basis functions used in the evaluation of corresponding MoM matrix entry. Writing the spatial-domain Green's function G_z^q in terms of its spectral-domain representation $\widetilde{G}_z^q$, followed by the change of the order of integrations, (2) can be cast into the following form

$$\left\langle \frac{\partial}{\partial x} T_x(x,y),\, G_z^q * \frac{\partial}{\partial z} B_z(y,z) \right\rangle = \iint dudv F_z^q(u,v,z=cons) \int dy B_z(y-v) \frac{\partial}{\partial x} T_x(x'+u, y) \quad (3)$$

where $x - x' = u$, $y - y' = v$ and

$$F_z^q \cong \frac{1}{4\pi} \int_{SIP} dk_\rho k_\rho H_0^{(2)}\left(k_\rho |\boldsymbol{\rho} - \boldsymbol{\rho}'|\right) \cdot GPOF\left\{ \int dz' \frac{\partial}{\partial z'} B_z(z') \widetilde{G}_z^q(k_\rho, z=cons, z') \right\} \quad (4)$$

Note that the auxiliary function $F_z(u,v)$ is obtained analytically in terms of complex exponentials and it is an explicit function of $u = x - x'$ and $v = y - y'$, and the inner integral of (3) can easily be obtained analytically for most basis and testing functions. Therefore, the same inner-product terms corresponding to other vertical strips can be obtained simply by evaluating $F_z(u,v)$ for different values of u and v, as long as the basis functions used to represent the current densities along them have identical z'-dependencies. Consequently, having more than one vertical conductors in a printed circuit would not require significant amount of additional computation.

The formulation described above is applied to a microstrip line lying along x-direction with four vertical y-spanning strips to assess and demonstrate the computational efficiency of the method. Here are the parameters of the microstrip line: the dielectric constant of the medium is 4.0; the length and width of the line is 18.0 cm and 0.1 cm, respectively; the thickness of the substrate is 0.4 cm; the frequency of operation is 2 GHz; and 71 horizontal basis functions along x-direction are employed. As the thickness of the substrate is uniform, which is usually the case for most of antenna and microwave applications, two basis functions are used over every vertical strip, and naturally they have the same z and z' dependencies, satisfying the only criterion for the efficiency of the method for multiple vertical strips. To validate the method, the current distribution along the microstrip line is first obtained, and compared to that from a commercially available EM simulation software, *em* by Sonnet, as shown in Fig. 1. An excellent agreement is observed; slight differences in the amplitude can be attributed to the inherent models of the approaches: *em* by Sonnet solves the problem in shielded environment while the method proposed here solves it in open environment, which inevitable causes some slight differences on the resonant frequencies of the structure.

Once the validation is complete, the computational efficiency of the proposed method is assessed in terms of the CPU time obtained from a 1.5 GHz Centrino CPU. The microstrip line is first analyzed with one vertical strip (at $x = 7.0$ cm), and then the number of vertical strips is increased to four by one-by-one. As the ultimate measure for the efficient handling of multiple vertical metallization, in addition to the first one, matrix fill time for additional vertical strips are listed in Table 1. For the matrix fill times in case I, the necessary auxiliary functions are calculated only once and used repeatedly, but for case II, the auxiliary functions are re-calculated for every entry corresponding to each basis and testing functions introduced with the addition of new vertical strips. It is observed that efficient use of auxiliary functions has significantly reduced the computational complexity of the whole method. This can be stated with adding new vertical strips to the microstrip line with one vertical strip costs about 4.0 seconds whereas it requires 70.0 seconds in case of not using auxiliary functions repeatedly. Note that CPU times are obtained by using only the symmetry of the MoM matrix and it has not been used any acceleration technique for the evaluation of MoM matrix entries.

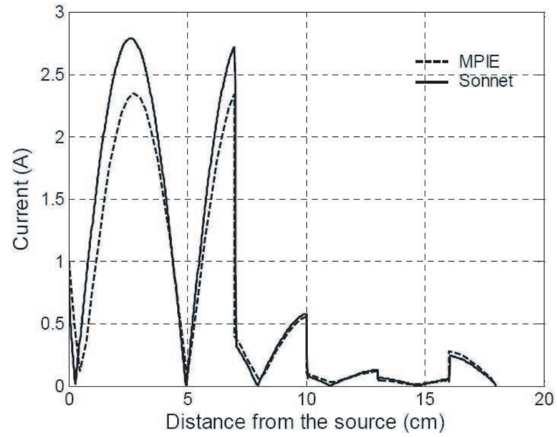

Figure 1: Magnitude of the current along the microstrip line with 4 vertical strips.

Table 1: MoM matrix fill times for each additional vertical strip.

Number of vertical strips	**MoM matrix fill-time (sec)**	
	CASE I	**CASE II**
1	11.8	69.8
2	4.0	68.6
3	4.1	72.2
4	4.2	75.8

4. Conclusions

Issues related to the implementation of DCIM have been first clarified, as it is used in conjunction with the MoM in the algorithm proposed in this paper. The algorithm, based on the DCIM-MoM technique, is assessed in terms of its accuracy and the efficiency in the analysis of printed geometries with multiple vertical conductors. It has been shown mathematically and numerically that, as long as the vertical dependencies of the basis or testing functions are chosen to be the same, the inclusion of additional vertical conductors is extremely efficient. Therefore, this approach seems to be a good candidate to use in conjunction with an optimization algorithm in a CAD tool.

REFERENCES

1. Mosig, J. R., "Arbitrarily shaped microstrip structures and their analysis with a mixed potential integral equation," *IEEE Trans. on Microwave Theory Tech.*, Vol. MTT-36, No. 2, 314–323, Feb. 1988.
2. Chow, Y. L., J. J. Yang, D. G. Fang, and G. E. Howard, "A closed-form spatial Green's function for the thick microstrip substrate," *IEEE Trans. on Microwave Theory Tech.*, Vol. 39, 588–592, March 1991.
3. Aksun, M. I., "A robust approach for the derivation of closed-form green's functions," *IEEE Trans. on Microwave Theory Tech.*, Vol. 44, No. 5, 651–658, May 1996.
4. Aksun, M. I. and G. Dural, "Clarification of issues on the closed-form Green's functions in stratified media," *IEEE Trans. Antennas Propagation*, Vol. AP-53, 3644–3653, Nov. 2005.
5. Chew, W. C., *Waves and Fields in Inhomogeneous Media*, IEEE PRESS Series on Electromagnetic Waves, New York, 1995.
6. Hua, Y. and T. K. Sarkar, "Generalized pencil-of-function method for extracting poles of an EM system from its transient response," *IEEE Trans. Antennas Propagat.*, Vol. 37, 229–234, Feb. 1989.
7. Kinayman, N. and M. I. Aksun, "Efficient use of closed-form green's functions for the analysis of planar geometries with vertical connections," *IEEE Trans. on Microwave Theory Tech.*, Vol. 45, 593–603, May 1997.

Thick Metal Models

J. C. Rautio
Sonnet Software, Inc., USA

Both the fine detail of fields at the edge of thick metal and the large scale fields over an entire circuit must be accurately represented in an EM analysis in order to correctly analyze thick metal in a planar circuit. This is a very difficult EM problem that has seen substantial research over the last decade. As a result, all serious commercial EM tools now include specialized thick metal models. The different models are briefly described and their relative advantages and disadvantages pointed out. Techniques for quantifying thick metal modeling error, as well as determining if a thick metal model is even needed, are detailed.

Analysis of Cylindrical Microstrip Line with Finite Thickness of Conductor

H. Miyagawa, **T. Nishikawa**, **K. Wakino**, **Y.-D. Lin**, **and T. Kitazawa**
Ritsumeikan University, Japan

Abstract—Novel analytical method based on extended spectral domain approach (ESDA) is presented for cylindrical microstrip line. The method utilizes the aperture fields as the source quantities, as opposed to the conventional methods, which have used the current on the strip as the source. The whole region can be divided into sub-regions by the introduction of aperture fields, and each sub-region can be treated independently. This method makes possible the analysis both of zero and finite thickness of the strip conductor. The numerical procedure incorporates the effects of the edge singularities properly and can afford the efficient and accurate calculations for the phase constants and characteristic impedances of a microstrip line with zero- and finite-thickness conductor. The calculated results by the present method reveal the effect of conductor thickness on the characteristics of a cylindrical microstrip line.

1. Introduction

Recently, curved surface substrates have attracted an attention as materials of antennas and front ends for portable terminals. A lot of analyses of the propagation characteristic of the stripline and the coplanar waveguide composed on a cylinder substrate are reported [1–6], including the moment method, the FDTD method [3], and the finite element method [5]. However, their works assumed the conductor thickness to be zero, and the report concerning the effect of the conductor thickness on the propagation characteristic has not be found. Recently, authors reported on the effect of the finite thickness of a conductor on electric characteristics of cylindrical coplanar waveguides (CCPWs) by using the extended spectral domain approach (ESDA).

In this paper, we report on the analytical method of the cylindrical microstrip line based on ESDA, and the effect of conductor thickness by numerical calculation. The present method utilizes the electric fields at the interface of the aperture as the source quantities, as opposed to the conventional methods [1, 2], which have used the current on the strip as the source. The accurate and efficient numerical procedure, which makes consideration for the field singularities near the conductor edge of zero- and finite-thickness, reveals the effect of the curvature and the finite thickness of a conductor on the characteristic impedances and the phase constants of the cylindrical microstrip line.

2. Theory

Cross section of a microstrip line on a cylindrical dielectric substrate is shown in Fig. 1(a). Curvature R of the cylindrical substrate is defined as the ratio of inner and outer diameter of substrate,

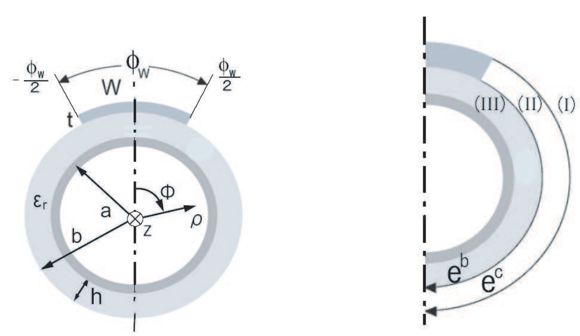

(a) Cross section. (b) Aperture fields.

Figure 1: Schematic structure of cylindrical microstrip line.

$$R = \frac{a}{b} = 1 - \frac{h}{b} \tag{1}$$

where $h = b - a$ is substrate thickness. A signal conductor of W in width is put on the substrate, which is backed by the ground conductor. Both conductors are assumed to be perfect electric conductor (PEC), but the signal conductor has the finite thickness t, as opposed to the previous reports. A single-layered substrate is assumed in the following explanation for the simplicity, although the method is applicable to multilayered and/or overlaid structure problem. The theoretical scheme is based on the ESDA [8–10]. The method has been successfully worked out to analyze the effect of the conductor thickness of the various types of planar transmission lines. Here, in this study, the method is extended further to the analysis of the effect of conductor thickness in cylindrical microstrip line. In the ESDA, first the aperture electric fields are introduced at the circumferential surfaces of dielectric substrate at $\rho = b$, $e^b(\phi)$, and the upper surface of signal conductor at $\rho = b + t$, $e^c(\phi)$ shown in Fig. 1(b). By introducing these aperture fields and utilizing the equivalence theorem, the whole region is divided into subregions, i. e., (I) the outer ($\rho > b + t$), (II) the aperture ($b < \rho < b + t$) and (III) the substrarte ($\rho < b$) subregions. After dividing the region, each subregion can be treated separately, and then the longitudinal components of electromagnetic fields in each subregion are expressed in terms of the appropriate eigenfunctions $\Phi_n^{(i)}(\phi)$, $\Psi_n^{(i)}(\phi)$, which satisfy the boundary conditions in the ϕ-direction.

$$E_z^{(i)}(\rho,\phi)e^{-j\beta z} = \sum_{n=0}^{\infty} \tilde{E}_z^{(i)}(\rho)\Phi_n^{(i)}(\phi)e^{-j\beta z} \tag{2}$$

$$H_z^{(i)}(\rho,\phi)e^{-j\beta z} = \sum_{n=0}^{\infty} \tilde{H}_z^{(i)}(\rho)\Psi_n^{(i)}(\phi)e^{-j\beta z} \tag{3}$$

$$i = I, II, III$$

where β is the unknown phase constant and $\tilde{E}_z^{(i)}$ is the transform of $E_z^{(i)}$. The transversal (ρ,ϕ) field components can be related to the longitudinal components $E_z^{(i)}$ and $H_z^{(i)}$ by utilizing the field equations. The general solution of the transform $\tilde{E}_z^{(i)}$ in region (i) can be expressed as

$$\tilde{E}_z^{(i)}(\rho) = A^{(i)}J_n(\beta_c\rho) + B^{(i)}Y_n(\beta_c\rho) \tag{4}$$

$$\beta_c = \sqrt{\omega^2\varepsilon\mu - \beta^2}$$

where $A^{(i)}$, $B^{(i)}$ is unknown constants, and they are determined by the boundary conditions at the interfaces. The continuities of electric fields are expressed as

$$E_\phi^{(III)}(\rho = a+0,\phi) = 0, \qquad E_z^{(III)}(\rho = a+0,\phi) = 0 \qquad \text{at} \ \ \rho = a \tag{5}$$

$$E_\phi^{(II)}(\rho = b+0,\phi) = E_\phi^{(III)}(\rho = b-0,\phi) = e_\phi^b \qquad \text{at} \ \ \rho = b \ \ (\frac{\phi W}{2} < \phi < \pi) \tag{6}$$

$$E_z^{(II)}(\rho = b+0,\phi) = E_z^{(III)}(\rho = b-0,\phi) = e_z^b \tag{7}$$

$$E_\phi^{(I)}(\rho = b+t+0,\phi) = E_\phi^{(II)}(\rho = b+t-0,\phi) = e_\phi^c \qquad \text{at} \ \ \rho = b+t \ \ (\frac{\phi W}{2} < \phi < \pi) \tag{8}$$

$$E_z^{(I)}(\rho = b+t+0,\phi) = E_z^{(II)}(\rho = b+t-0,\phi) = e_z^c. \tag{9}$$

These continuity conditions are transformed into spectral domain and they are used to relate the unknowns $A^{(i)}$, $B^{(i)}$ to the aperture fields. The fields are then related to the aperture fields as follows

$$E^{(II)}(\rho,\phi) = \int_{\phi'} \{\overline{\overline{T}}^{(II)}(b,\phi|b+t,\phi')\cdot\mathbf{e^c}(\phi') + \overline{\overline{T}}^{(II)}(b,\phi|b,\phi')\cdot\mathbf{e^b}(\phi')\}d\phi' \tag{10}$$

$$H^{(II)}(\rho,\phi) = \int_{\phi'} \{\overline{\overline{Y}}^{(II)}(b,\phi|b+t,\phi')\cdot\mathbf{e^c}(\phi') + \overline{\overline{Y}}^{(II)}(b,\phi|b,\phi')\cdot\mathbf{e^b}(\phi')\}d\phi' \tag{11}$$

where, $\overline{\overline{T}}'_s$, $\overline{\overline{Y}}'_s$ are the dyadic Green's functions. Then, the integral equations on the aperture fields are obtained by using the continuities of magnetic fields at the aperture surfaces,

$$H_\phi^{(II)}(\rho = b + 0, \phi) = H_\phi^{(III)}(\rho = b - 0, \phi) \qquad (\frac{\phi W}{2} < \phi < \pi) \tag{12}$$

$$H_z^{(II)}(\rho = b + 0, \phi) = H_z^{(III)}(\rho = b - 0, \phi) \tag{13}$$

$$H_\phi^{(I)}(\rho = b + t + 0, \phi) = H_\phi^{(II)}(\rho = b + t - 0, \phi) \qquad (\frac{\phi W}{2} < \phi < \pi) \tag{14}$$

$$H_z^{(I)}(\rho = b + t + 0, \phi) = H_z^{(II)}(\rho = b + t - 0, \phi). \tag{15}$$

Applying the Galerkins procedure to these integral equations, we get the determinant equation for the phase constant β. In the Galerkins, the unknown aperture fields are expressed in terms of the appropriate basis functions $\xi_{\phi i}(\phi)$ and $\xi_{zi}(\phi)$ as,

$$e_\phi^b(\phi) = \sum_{i=1}^{N} b_{\phi i}\xi_{\phi i}(\phi), \qquad e_z^b(\phi) = \sum_{i=1}^{N} b_{zi}\xi_{zi}(\phi) \tag{16}$$

$$e_\phi^c(\phi) = \sum_{i=1}^{N} c_{\phi i}\xi_{\phi i}(\phi), \qquad e_z^c(\phi) = \sum_{i=1}^{N} c_{zi}\xi_{zi}(\phi) \tag{17}$$

where $b_{\phi i}$, b_{zi}, $c_{\phi i}$, and c_{zi} are the unknown expansion coefficients. The basis functions $\xi_{\phi i}(\phi)$, $\xi_{zi}(\phi)$, which incorporate the singularities of fields properly near the conductor edge [8–10], are used in the following computations. For the case with the conductors of zero thickness, the aperture region (II) will be eliminated in the procedure and the aperture field e^b equals to e^c.

The definition of the characteristic impedance is somewhat ambiguous for the hybrid mode propagation along microstrip line. We adopt the voltage-current definitions

$$Z_{VI} = \frac{V_o}{I_o} \tag{18}$$

where V_o is the voltage between the center strip and the ground conductor, and I_o is the total current flowing in the z-direction on the strip conductor. The voltage V_o is evaluated by integrating the radial component of electric field $E_\rho^{(III)}$ between the ground ($\rho = a$) and the signal ($\rho = b$) conductors,

$$V(\phi) = \int_a^b E_\rho(\rho, \phi)d\rho \tag{19}$$

where ϕ may be any in $0 < \phi < \phi_W/2$. Therefore $V(\phi)$ is integrated with ϕ over $0 < \phi < \phi_W/2$ to get

$$V_o = \frac{2}{\phi_W}\int_0^{\frac{\phi_W}{2}} V(\phi)d\phi. \tag{20}$$

The current I_o can be evaluated by the line integral C of the magnetic field around the strip conductor [7]

$$I_o = \oint_c \mathbf{H} \cdot dl. \tag{21}$$

3. Numerical Procedure and Results

The conventional methods have treated the propagation characteristics of a microstrip line on a cylindrical substrate assuming the conductor thickness to be zero [2]. The present method, when the aperture field is adopted as the source quantity in the formulation, can afford to present the characteristics of the case with finite as well as zero thickness. Also, the present formulation procedure could employ the current on the strip instead of the aperture field as the source quantity, although this procedure could be applied only to the case with zero thickness. Fig. 2 shows the frequency dependency of the effective dielectric constant ε_{eff} and the characteristic impedance Z_{VI} of a microstrip line on a cylindrical substrate with larger R [2]. The effective dielectric constant ε_{eff} is obtained in terms of the phase constant β as

$$\varepsilon_{eff} = \{\beta/\omega\sqrt{\varepsilon_0\mu_0}\}^2 \tag{22}$$

The results of zero thickness conductors are calculated by both the aperture field and the current bases, and both results are in excellent agreement and they agree well with the conventional ones [2] over the frequencies. The figure includes the results of the case with finite thickness of the strip conductor (50 μm) showing the effects of the conductor thickness on ε_{eff} and Z_{VI}.

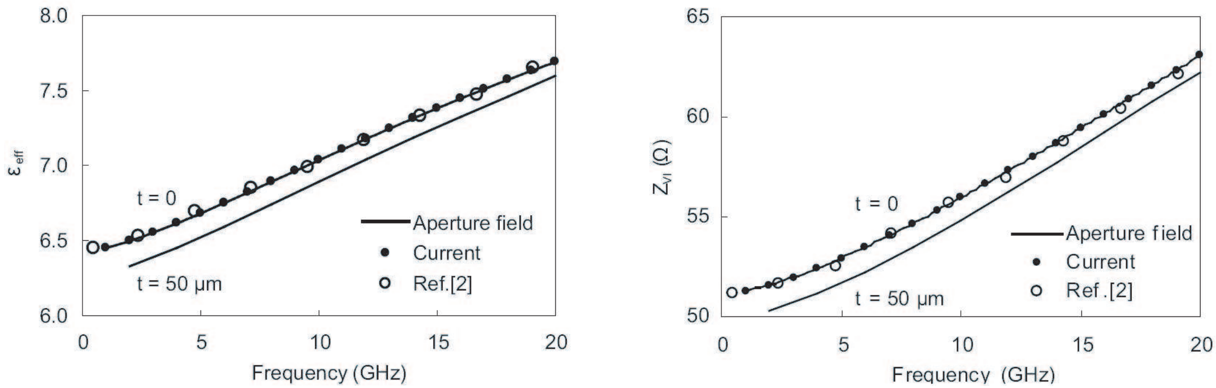

(a) ε_{eff}. (b) Z_{VI}.

Figure 2: Frequency dependency of propagation characteristics. $\varepsilon_r = 9.6$, $h = 1\,mm$, $W = 1\,mm$, $R = 0.9$.

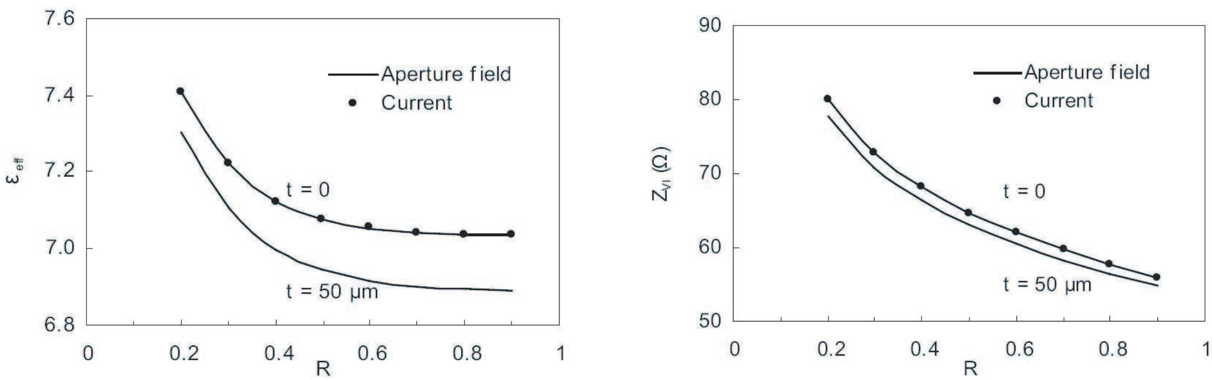

(a) ε_{eff}. (b) Z_{VI}.

Figure 3: Curvature dependency of propagation characteristics. $\varepsilon_r = 9.6$, $h = 1\,mm$, $W = 1\,mm$, $f = 10\,GHz$.

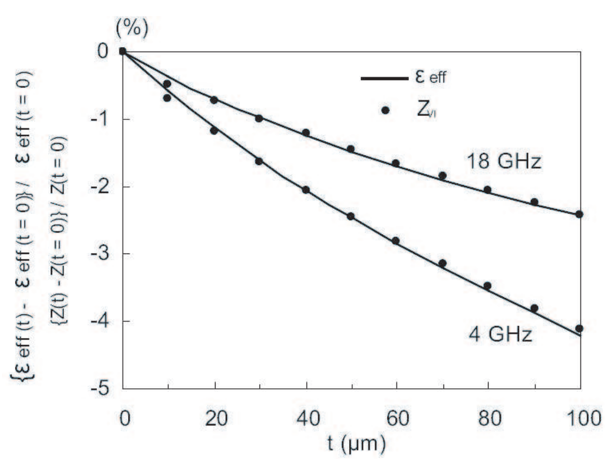

Figure 4: Thickness effect on propagation characteristics. $\varepsilon_r = 9.6$, $h = 1\,mm$, $W = 1\,mm$, $R = 0.9$.

The present methods is equally applicable to the a cylindrical microstrip line with larger and smaller curvature rate R. Fig. 3 shows the curvature dependency of ε_{eff} and Z_{VI}. The value of ε_{eff} increases rapidly when curvature rate R is 0.5 or less. That is, the concentration of the electromagnetic field in the dielectric substrate becomes stronger as the curvature ratio becomes smaller. Therefore, the effect of the thickness of the conductor becomes smaller for the smaller R. Fig. 4 shows the conductor thickness effect where the relative changes of ε_{eff} and Z_{VI} are presented with the thickness variation of conductor. Both ε_{eff} and Z_{VI} are decrease monotonously up to 100 μm thickness conductor. It should be noted that the effect of the conductor thickness becomes smaller for higher frequency ($f = 18$ GHz), as opposed to a cylindrical coplanar waveguides (CCPWs), where the effect becomes larger for higher frequency. This is why the electromagnetic field concentrates more in the dielectric substrate between the strip and the ground conductors and the effect of conductor thickness becomes smaller for higher frequency.

4. Conclusion

Novel analytical method based on extended spectral domain approach (ESDA) is presented for a cylindrical microstrip line. The method is able to treat the effect of the finite thickness of a strip conductor by utilizing the aperture electric fields as source quantities. The numerical procedure incorporates the effects of the edge singularities properly and can afford the efficient and accurate calculation method for the characteristic impedances in addition to the phase constants of a cylindrical microstrip line. The calculated results for zero-thickness conductor by both procedures, based on current or aperture field, are in good agreement and also they agree well with the published data. The results obtained by the present method show the curvature dependency of the propagation characteristics and reveal the effect of conductor thickness, which is different from that of a cylindrical coplanar waveguides (CCPWs).

REFERENCES

1. Alexopoulos, N. G. and A. Nakatani, "Cylindrical substrate microstrip line characterization," *IEEE, Trans. Microwave Theory Tech.*, Vol. 35, No. 9, 843–849, 1987.
2. Nakatani, A. and N. G. Alexopoulos, "Coupled microstrip lines on a cylindrical substrate," *IEEE Trans. Microwave Theory Tech.*, Vol. 35, No. 12, 1392–1398, 1987.
3. Dib, N., T. Weller, M. Scardelletti, and M. Imparato, "Analysis of cylindrical transmission lines with the finite-difference time-domain method," *IEEE, Trans. Microwave Theory Tech.*, Vol. 47, No. 4, 509–512, 1999.
4. Su, H.-C. and K.-L. Wong, "Dispersion characteristics of cylindrical coplanar waveguides," *IEEE, Trans. Microwave Theory Tech.*, Vol. 44, No. 11, 2120–2122, 1996.
5. Kolbehdari, M. A. and M. N. O. Sadiku, "Finite & Infinite element analysis of coupled cylindrical microstrip line in a nonhomogeneous dielectric media," *Proc. IEEE Southeastcon '95.*, 269–273, 1985.
6. Simons, R. N., "Coplanar waveguide circuits, components, and systems," *Wiley-Interscience*, 2001.
7. Yamamoto, H., H. Miyagawa, T. Nishikawa, K. Wakino, and T. Kitazawa, "Full wave analysis for propagation characteristics of cylindrical coplanar waveguides with finite thickness of conductor," *Microwave Theory Tech.*, Vol. 53, No. 6, 2187–2195, 2005.
8. Kitazawa, T. and T. Itoh, "Propagation characteristics of coplanar-type transmission lines with lossy media," *IEEE Trans. Microwave Theory Tech.*, Vol. 39, No. 10, 1694–1700, 1991.
9. Kitazawa, T., "Analysis of shielded striplines and finlines with finite metallization thickness containing magnetized ferrites," *IEEE Trans. Microwave Theory Tech.*, Vol. 39, No. 1, 70–74, 1991.
10. Kitazawa, T., "Nonreciprocity of phase constants, characteristic impedances and conductor losses in planar transmission lines with layered anisotropic media," *IEEE Trans. Microwave Theory Tech.*, Vol. 43, No. 2, 445–451, 1995.